Applied Surface Science 542 (2021) 148661

Contents lists available at ScienceDirect

Applied Surface Science

journal homepage: www.elsevier.com/locate/apsusc

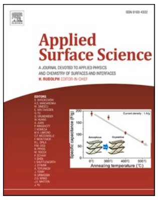

Full Length Article

Functional separator for promoting lithium ion migration and its mechanism study

Xin Wang [a], Haiming Hua [a], Longqing Peng [a], Boyang Huang [a], Peng Zhang [b,*], Jinbao Zhao [a,*]

[a] *State Key Laboratory of Physical Chemistry of Solid Surfaces, Collaborative Innovation Centre of Chemistry for Energy Materials, State-Province Joint Engineering Laboratory of Power Source Technology for New Energy Vehicle, Engineering Research Center of Electrochemical Technology, Ministry of Education, College of Chemistry and Chemical Engineering, Xiamen University, Xiamen 361005, PR China*

[b] *College of Energy & School of Energy Research, Xiamen University, Xiamen 361102, PR China*

ARTICLE INFO

Keywords:
Lithium ion battery
TiO_2
Oxygen vacancies
Lithium ion transference number
Interaction

ABSTRACT

TiO_2 nanoparticles with oxygen vacancies (B-P25) prepared by $NaBH_4$ reduction method were coated onto PE separator to construct an active ceramic layer. The effect of the functional layer was carefully studied especially the interaction between oxygen vacancies on B-P25 and species in the liquid electrolyte. The B-P25 not only improves the affinity between the separator and electrolyte, but also improves the lithium ion transference number of the electrolyte, from 0.28 to 0.50. Based on the infrared spectroscopy results, it was found that B-P25 weakened the coordination between Li^+ and EC, and partially desolvated the Li^+-EC complex. Further theoretical calculation showed that the oxygen vacancies are more likely to adsorb EC molecules and indirectly promote the dissociation of Li^+-EC, so that partially solvated Li^+ has a stronger mobility and a higher lithium ion conductivity in the electrolyte. Therefore, B-P25 as an active layer assembled in $LiFePO_4$ half-cell has better rate performance.

1. Introduction

Lithium-ion batteries (LIBs) as an excellent electrical energy storage device have facilitated our daily live and society development, such as mobile communications, green travel as well as clean energy like wind farm integration to grid [1,2]. In order to pursue higher energy or power density of LIBs, high-voltage ternary cathode materials are eagerly looking forward to be applied. However, due to the instability, it is easily to cause side reactions with electrolyte especially in improper operation or high temperature environment, which has a high probability of inducing heat accumulation, finally leading to thermal runaway and serious safety accidents. As an important part of LIBs, separator with improving the thermal stability is beneficial to the safety of the cell. At present, the most common strategy is to coat the commercial polyolefin separators with high temperature resistant oxide ceramics (usually named ceramic coated separators), which can inhibit the thermal shrinkage of the polymer materials relying on the size stability of ceramic particles under high temperature conditions. In this regard, Al_2O_3 [3], TiO_2 [4], SiO_2 [5], boron nitride [6] with different morphology such as particle, nanotube, nanowire have been reported in the articles as functional layers to improve the thermal stability of polyolefin separators.

It is not limited to simply improving the dimensional stability of the separator, and endowing the separator with more functions is also a research hotspot. Therefore, many researchers have constructed organic functional layers on the surface of oxide, which not only improves the thermal stability of the separator, but also enhances the affinity between the separator and electrolyte. Some special organic functional layers can also enhance the interaction between the separator and the electrolyte, so as to improve the lithium ion transference number (t_{Li^+}) and lithium ion conductivity, or inhibit the generation of HF. For example, our research group have grown polymethyl methacrylate (PMMA) organic shell on the surface of SiO_2 to enhance the affinity of the separator and electrolyte by one common gel polymer electrolyte matrix PMMA, and the liquid retention capacity of the separator is also increasing [7]. We also constructed a thin layer of polydopamine (PDA) in situ on the ceramic coated separator not only further improved the thermal stability, but also enhanced the wettability with the electrolyte by introducing the polar group (–OH, –NH–) of polydopamine [8]. It's reported that the amino functionalized SiO_2 was coated on the separator, which exhibit good wettability and high ionic conductivity. The amino functionalized SiO_2 serving as Lewis base can effectively complex with thermally decomposed PF_5, thereby preventing hydrolysis to produce HF [9]. In addition, it has been reported that polyacrylic acid [10],

---

* Corresponding authors.
E-mail addresses: pengzhang@xmu.edu.cn (P. Zhang), jbzhao@xmu.edu.cn (J. Zhao).

https://doi.org/10.1016/j.apsusc.2020.148661
Received 16 September 2020; Received in revised form 9 November 2020; Accepted 29 November 2020

polyethyleneimine [11,12] and other functional polymers are applied to modify the separator through layer by layer self-assembly process to enhance the interaction between the separator and electrolyte, and thus increase the t_{Li^+}, so as to improve the lithium ion conductivity.

Just as the organic modification carried out on the ceramic separator, it is indeed conducive to the electrolyte affinity of the separator, and the t_{Li^+} increased, but there is a problem of tedious process. As a result, the surface defect modification of oxide ceramics directly is an attractive scheme. The newly introduced defects will increase the interaction sites or enhance the interaction with electrolyte to improve the conductivity, Li^+ migration ability and other properties. As well known to all, the basic physical and chemical properties of oxide materials are seriously affected by their defect structure [13]. For example, the introduction of defects can improve the absorbance of TiO_2 [14], and the defect sites can be used as the active sites to enhance catalytic activity [15,16]. Therefore, it is feasible and innovative to directly modify the oxide ceramic defects while avoiding the tedious organic modification in the later process.

In this paper, we have chosen titanium dioxide (TiO_2) as the ceramic coating material, because TiO_2 is a kind of common oxide semiconductor materials and there are many methods to introduce oxygen vacancies on its surface reported in the literature [16–20]. The commercial TiO_2 nanomaterial P25, due to its small particle size and large specific surface area, is conducive to full contact with the electrolyte. And TiO_2 with oxygen vacancies was prepared by the $NaBH_4$ reduction method [17,18,20]. It was also coated on the separator as an active layer to explore the interaction of defect-modified TiO_2 with the electrolyte, and we have tried to explain how oxygen vacancy defects affect the electrolyte with theoretical calculations. It provides an effective method to develop functional separators for LIBs with both the improved safety and electrochemical performance.

2. Experimental section

2.1. Experiment procedure

The commercial P25 nanomaterial was purchased from Evonik Deguss company, whose particle size is about 21 nm combined with specific surface area around $50 \pm 15\ m^2/g$. P25 was used to prepare the TiO_2 nanoparticles with oxygen vacancies (abbreviated as B-P25) by $NaBH_4$ reduction method [17,18,20]. Firstly, P25 was uniformly mixed with an equal mass of $NaBH_4$, heated to 350 °C for 1 h under argon atmosphere, centrifuged repeatedly three times with deionized water to remove residual $NaBH_4$ and then B-P25 with oxygen vacancies was gained. Secondly, P25 and B-P25 were respectively coated on the polyethylene (PE) separator (Jinhui Hi-Tech Optoelectronic Materials Co., Ltd.), carboxymethyl cellulose as well as styrene-butadiene rubber was used as the composite binder, and the mass ratio of oxide and binder was controlled at 9:1 [3]. After vacuum dried at 60 °C for 24 h, the coated separator was obtained, and was marked as P25@PE and B-P25@PE separators.

2.2. Characterization

The morphology of commercial P25 nanomaterials was characterized by Transmission Electron Microscope (Bk TEM Tecnai F30). The crystal structure information of TiO_2 with oxygen vacancies was characterized by X-ray powder diffraction (RigakuMiniFlex 600). X-ray photoelectron spectroscopy (PHI, Quantum 2000) was used to analyze the surface chemical composition of TiO_2. The surface and cross-sectional morphology of the P25@PE and B-P25@PE separators were observed by field scanning electron microscopy (FE-SEM, S-4800, Hitachi). The interaction of liquid electrolyte with B-P25 was characterized by attenuated total reflection (ATR) using a Nicolet IS5 spectrometer (ThermoFisher Scientific Inc.). The affinity of the P25@PE and B-P25@PE separators to the electrolyte was characterized by a contact angle instrument (Powereach JC2000C1). After the separator was fully wetted by the electrolyte, the proportion of the mass difference before and after the separator to the mass of the original separator was calculated as the electrolyte uptake of the separator. The ionic conductivity (σ) was measured from the AC impedance method, and the separator immersed in electrolyte was assembled in a stainless steel symmetrical cell to test bulk resistance (R_b) on an electrochemical workstation (CHI660E, Chenhua). The specific ionic conductivity was calculated as follows: $\sigma = l/(R_b \times A)$, where A is the area of the stainless steel electrode ($2\ cm^2$), l is the thickness of separator. The t_{Li^+} of the separator was measured by steady current and AC impedance method [21]. The separator immersed in electrolyte was assembled in a lithium symmetric cell and the t_{Li^+} was calculated according to the following formulas:

$$t_{Li^+} = \frac{I_s(\Delta V - I_0 R_0)}{I_0(\Delta V - I_s R_s)}$$

where I_0 and I_s are the initial and steady state current; ΔV is the applied constant potential difference (10 mV); R_0 and R_s are the interface impedance before and after polarization.

In order to evaluate the electrochemical performance of P25@PE and B-P25@PE separators, we assembled them in the half-cell, in which lithium iron phosphate ($LiFePO_4$, Taiwan Likai Co., Ltd.,) positive pieces according to the $LiFePO_4$/acetylene black/PVDF mass ratio of 8/1/1 were coated on aluminum foil with a loading of approximately 2.1 mg/cm^2 and a diameter of 12 mm. The electrolyte was 1 M $LiPF_6$ dissolved in ethylene carbonate (EC) and diethyl carbonate (DEC) solvents with volume ratio of 1:1. The cycle performance test of the cells was tested by galvanostatic charge/discharge testing at a 1C current density on NEWARE battery testing instrument, voltage curve 2.5–3.8 V. Coin-type cells were all assembled in an Ar-filled glove box (Mbraun, Germany).

2.3. Computational details

Density functional theory (DFT) calculations were performed using Gaussian09 E01 software [22,23]. The geometries of PF_6^- and EC were optimized using B3LYP-D3 density functional with def2-SVP basis set. Single point energy of all optimized geometries was further calculated with def2-TZVP basis set. The continuum solvation model SMD was used to calculate energy of dissolution in EC/DEC electrolyte. The relative dielectric constant(ε) of the electrolyte was 46.4 and parameters of non-polar parts were same as ethyl ethanoate. The cluster taken from the [1 1 0] crystal face of anatase was used as a model of the titanium site. eight H atoms were added to the cluster to maintain the electrical neutrality. Restrictive optimization (only H atoms are optimized) was used to the cluster. In the subsequent interaction calculations, the geometry of titanium cluster remained frozen and only the geometries of anions were optimized. The visualization of geometries and ESP were performed using CYLview software.

3. Results and discussion

3.1. Oxygen vacancies confirmation

According to related literature reports [17,20], we have prepared TiO_2 nanoparticles with oxygen vacancies by $NaBH_4$ reduction method. In the P25 and B-P25 high-resolution electron microscopy images (Fig. 1a and 1b), no apparent changes are observed in the morphology of B-P25 nanoparticles after $NaBH_4$ treatment of P25.

X-ray photoelectron spectroscopy (XPS) is used to character the composition and chemical state of sample of P25 and B-P25 to determine the presence of defect such as Ti^{3+} and oxygen vacancies formed on the surface. In Fig. 1c, the typical peaks of Ti $2p_{3/2}$ and Ti $2p_{1/2}$ were 458.7 eV and 464.4 eV respectively in P25, however, in B-P25, the Ti 2p correlation peaks moved to 458.2 eV and 463.9 eV, indicating that Ti^{3+} was introduced in B-P25 after $NaBH_4$ reduction, which is generally

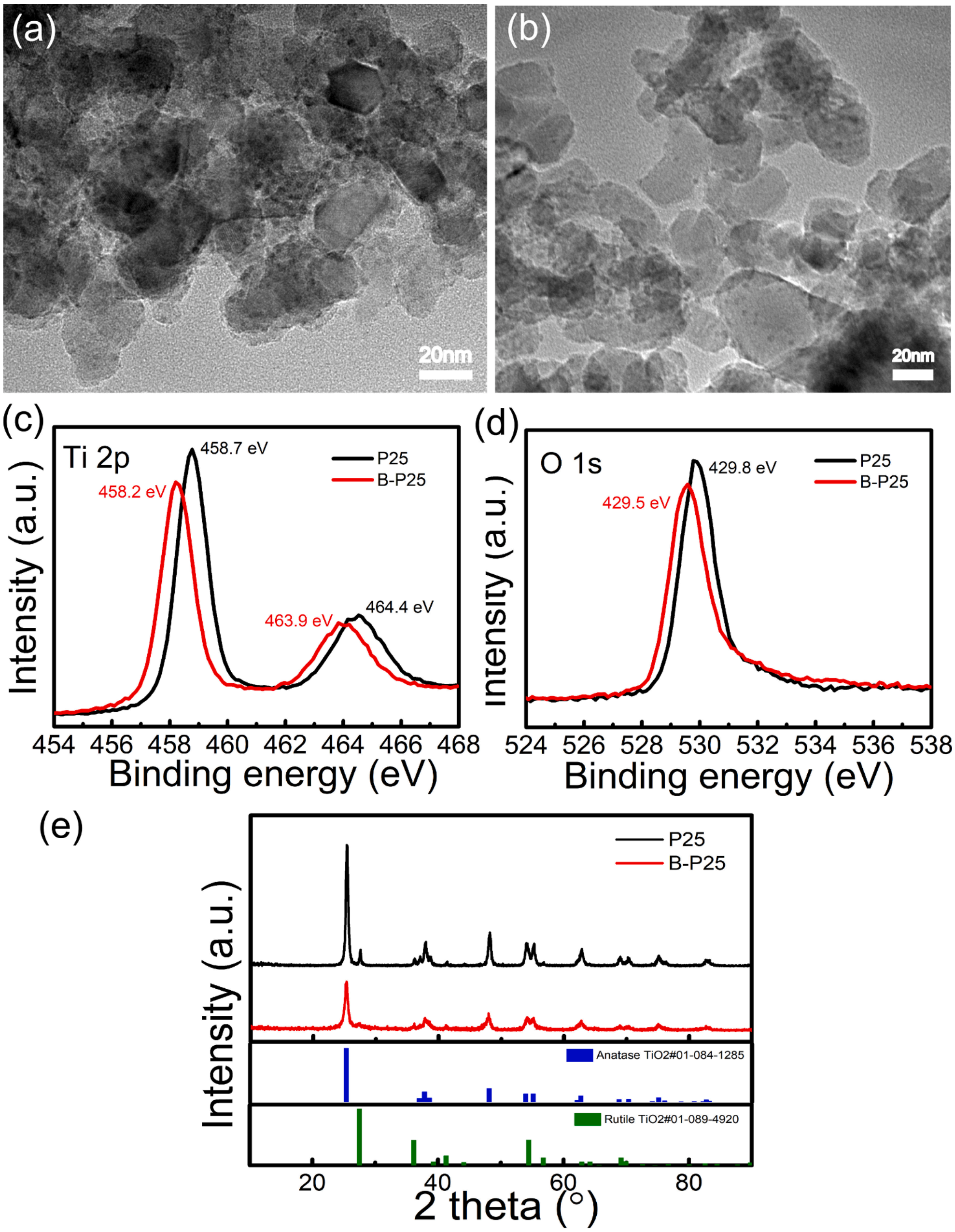

Fig. 1. (a) and (b) are P25 and B-P25 electron micrographs; (c) and (d) are the XPS spectra of the Ti 2p and O 1s orbitals of P25 and B-P25, respectively; (e) are the XRD pattern of P25 and B-P25.

accompanied by the generation of oxygen vacancies [16,18,20]. We also have observed a similar shift in O 1s XPS profiles shown in Fig. 1d, which is in agree with the transfer of electrons to the neighboring oxygen vacancies [17,18]. Besides from the structure analysis of the X-ray diffraction patterns of P25 and B-P25 in Fig. 1e, it can be known that commercial P25 is a mixture of anatase (JCPDS No. 01-084-1285) and rutile phase (JCPDS No. 01-089-4920) TiO_2, after high temperature reduction by $NaBH_4$, black TiO_2 containing oxygen vacancies is produced. It can be distinguished from XRD pattern that no new diffraction peak is generated. However, the diffraction intensity of B-P25 decreases, indicating that the disorder of the crystal structure increases. Combing the characterization of XRD and XPS, B-P25 nanomaterial with oxygen vacancies has been successfully prepared.

3.2. *Structure and properties*

The scanning electron microscopy images of Fig. 2 show that the pristine PE separator surface is porous structure (Fig. 2a), and the P25 and B-P25 nanoparticles are densely coated on the PE separator (Fig. 2b and 2c) without obvious micro-pores. According to the cross sectional images (Fig. 2d and 2e), the ceramic layer is about 6 μm in thickness. Through the observation of the morphology, we have successfully coated P25 and B-P25 nanoparticles onto the PE separator, namely, the P25@PE and B-P25@PE separators were prepared.

The lithium ion transference number (t_{Li^+}) represents the ratio of cations (Li ions) transfer charge in the electrolyte to the total charge of both anions and cations. The migration of Li^+ in traditional electrolyte was slowed down due to the solvation of Li^+ with EC molecules. Generally, the t_{Li^+} of electrolyte with $LiPF_6$ as lithium salt in pristine PE separator is 0.2–0.4 [24,25]. Increasing the t_{Li^+} is beneficial to reduce

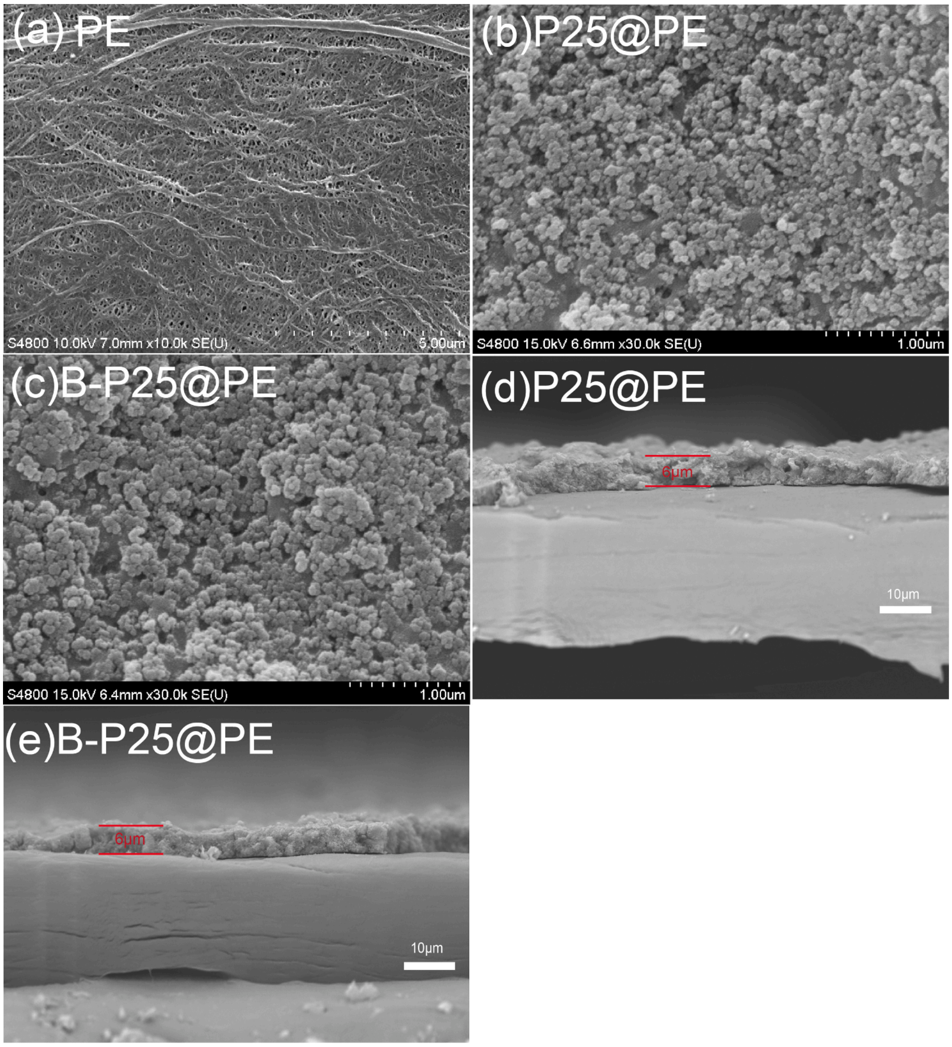

Fig. 2. (a) Surface morphology of the original PE separator; (b) and (c) are the surface morphology of the P25@PE and B-P25@PE separators, respectively; (d) and (e) are the cross-sectional profiles of the P25@PE and B-P25@PE separators, respectively.

the concentration polarization of the electrode as well as prevent the side reaction at the electrolyte/electrode interface [11,26]. By measuring the change of t_{Li^+}, we can preliminarily judge whether there is an interaction between the introduced active nano-oxides and the electrolyte. By combining steady-state current with AC impedance, we measured the t_{Li^+} in lithium-symmetric batteries with PE, P25@PE and B-P25@PE separators. As shown in Fig. 3a-c, the electrolyte was infiltrated in the ordinary separator, and the t_{Li^+} is only 0.28, which is consistent with other reports [12,24,25]. It is because the migration ability of PF_6^- is better than the solvated Li^+ ion thus contributing a large part of the whole ionic conduction. However, only Li ions participate in the electrochemical reaction namely intercalation and de-intercalation process which could provide the foundation of the energy conversion. Introducing the P25 oxide active layer, the t_{Li^+} increased to 0.39, which may be due to the Lewis acid sites on the surface of the nano-oxide P25, which can trap PF_6^- and limit its movement [10,27]. Introducing the B-P25 oxide active layer, the t_{Li^+} is increased to 0.50, which may be that oxygen vacancies change the migration ability of anions and cations in the electrolyte, either restrict the movement of anion PF_6^- or accelerate the migration of Li^+. In order to explore the reasons for the change, we analyzed the oxide active layer after the electrolyte infiltration by ATR spectrum.

As shown in Fig. 4a, the peak at 846 cm^{-1} is assigned to the P-F stretching of free PF_6^- anion [28–30]. Comparison shows that no matter the introduction of the P25 or B-P25 active layer, the peak position of PF_6^- does not shift very much, basically exclude the interaction of P25 and B-P25 on PF_6^-. The lithium salt ($LiPF_6$) is dissolved in the ester electrolyte, Li^+ ions are solvated by the EC molecules and formed $C = O{\cdot\cdot}Li^+$ coordination bond, and accordingly the mobility of Li^+ decreases after solvation. In Fig. 4b, the characteristic peaks ascribed to the ring bending modes of free EC (716 cm^{-1}) and Li^+ associated EC (Li^+-EC) (729 cm^{-1}) are identified [30,31]. According to the ratio of correlation peak areas ($A_{Li+\text{-EC}}/A_{\text{free EC}}$), the values of PE, P25@PE and B-P25@PE separators soaked with electrolyte are 1.40, 1.34 and 1.29, respectively. It is worth noting that the degree of solvation of Li^+ and EC molecules decreases gradually after the introduction of the active layer, especially the oxygen vacancies at the surface can significantly weaken the solvation of Li^+, so that the partially solvated Li^+ has a faster migration ability.

In order to further insight the mechanism at the molecular level, the adsorption of PF_6^- ion and EC molecules on the TiO_2 oxygen defect model under solution environment was studied by quantum chemistry. The surface of the oxygen-deficient structure exposes the Ti atom of the unsaturated ligand, which has a strong positive charge and can bind the lone pair of electrons on the carbonyl oxygen of the EC molecule or the PF_6^- ion fluorine atom. The adsorption structure is shown in Fig. 5. The calculation results show that the binding energy between EC and the model is −19.3 kcal/mol, and the binding energy between PF_6^- and the

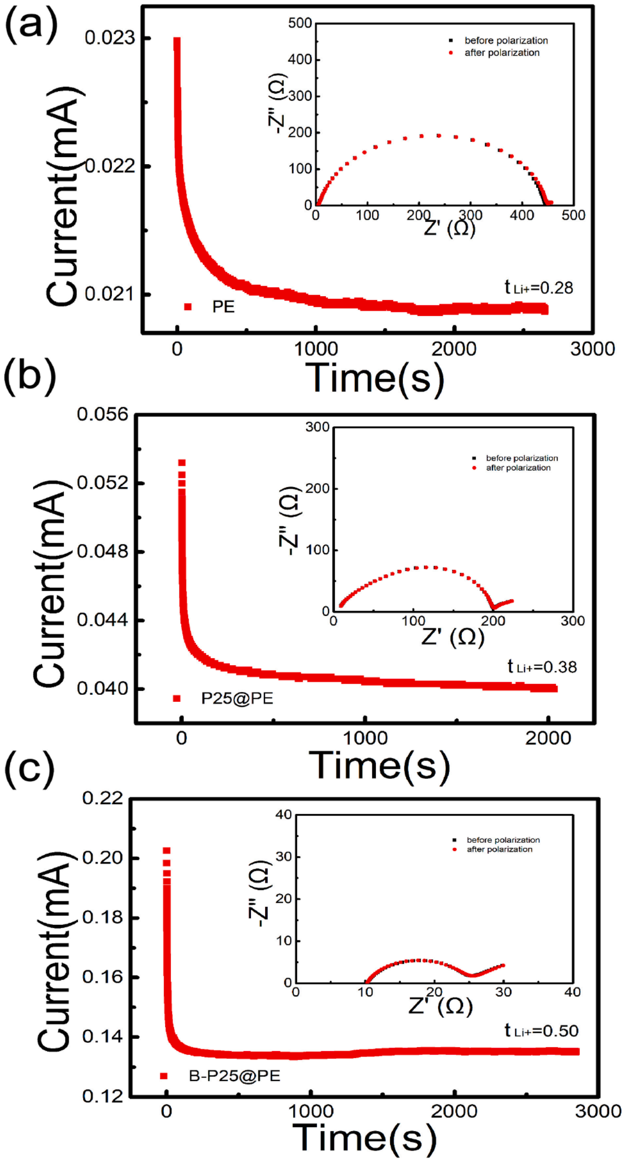

Fig. 3. (a), (b) and (c) are the steady-state current curves of PE, P25@PE and B-P25@PE separators assembled in lithium symmetric cells, respectively. The internal picture is the AC impedance spectrum before and after polarization.

model is −8.8 kcal /mol. The former has a much stronger binding tendency than the latter, and the concentration of EC molecules in the solution is much greater than PF$_6^-$, so the oxygen-deficient Ti atoms are mainly combined with EC molecules, and the results of infrared spectroscopy also confirms this.

The separator has the function of isolating electron and conducting ions. Ionic conductivity is an important performance parameter of separator. The interfacial impedance of different separators in stainless steel symmetrical cells was tested based on the AC impedance method (Fig. 6a). The ionic conductivity of PE, P25@PE and B-P25@PE separators are 0.43, 0.54 and 0.53 mS·cm^{-1}, respectively. The addition of TiO$_2$ nanoparticles increases the wettability and electrolyte uptake of the PE pristine separator, making lithium ions more easily transport through the separator.

The electrochemical stability of modified separators was evaluated by linear sweep voltammetry method, the results are displayed in Fig. 6b, the electrochemical windows of P25@PE and B-P25@PE separators are similar to those of PE separator, indicating that P25 and B-P25 nanoparticles don't seriously affect the electrochemical stability of PE separator. So, the modification of oxygen vacancies in TiO$_2$ has no adverse effect on ionic conductivity and electrolyte uptake, and also has better affinity.

The conduction of ions is inseparable from the electrolyte filling the separator, thus, good infiltration between separator and electrolyte is conducive to lithium ion migration in electrolyte. Therefore, we have tested the contact angle between PE, P25@PE and B-P25@PE separators and electrolyte, as shown in Fig. S1a, electrolyte (LiPF$_6$ dissolved in EC/DEC) showed good wettability to PE, P25@PE and B-P25@PE separators with value of 33°, 9.6° and 0°. The contact angle decreases with the addition of ceramic layer, which is due to the hydroxyl groups on the ceramic surface, which is also consistent with the other reports [3,32]. Moreover, B-P25 has better affinity with electrolyte than P25, which may be the role of oxygen vacancies. Subsequently, we have tested the electrolyte uptake of PE, P25@PE and B-P25@PE separators. By calculating the percentage of electrolyte absorbed by separator to the mass of the separator, we obtained that the electrolyte uptake of PE, P25@PE and B-P25@PE separators were 85%, 133% and 135%, respectively. The increase of the electrolyte uptake may be mainly due to the good affinity between the ceramic layer and the electrolyte.

The thermal stability of the separator is also an important property, which can prevent the short circuit of the battery caused by the shrinkage of the separator at high temperature. Since the melting point of the PE separator is about 130 °C, we tested the thermal stability of the separator at different temperatures (30 °C, 130 °C, 150 °C) (Fig. S1b). The pristine PE separator shrunk at 130 °C, and shrinkage was more serious at 150 °C. On the contrary, the P25@PE and B-P25@PE separators had good thermal stability at 150 °C due to the existence of ceramic layer [3,8]. From the photos, it can be found that the dimensional stability of P25@PE and B-P25@PE was not obviously different.

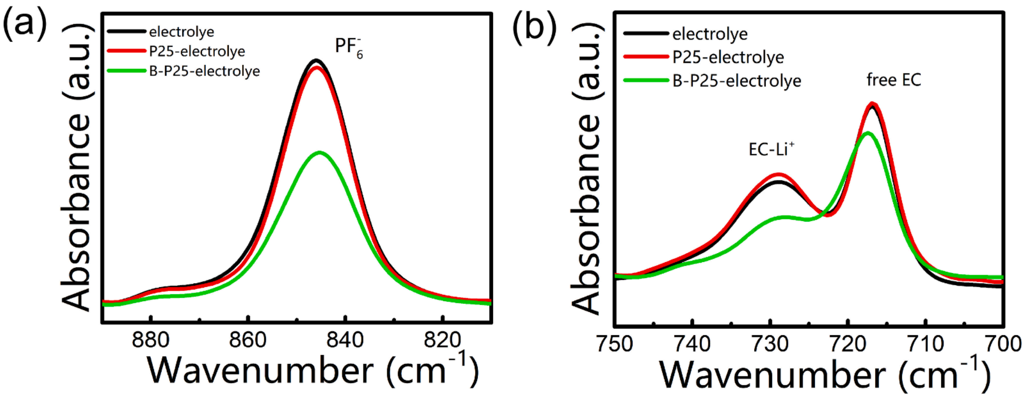

Fig. 4. (a) and (b) are ATR spectrum of P25@ PE and B-P25@PE separators soaked in electrolyte.

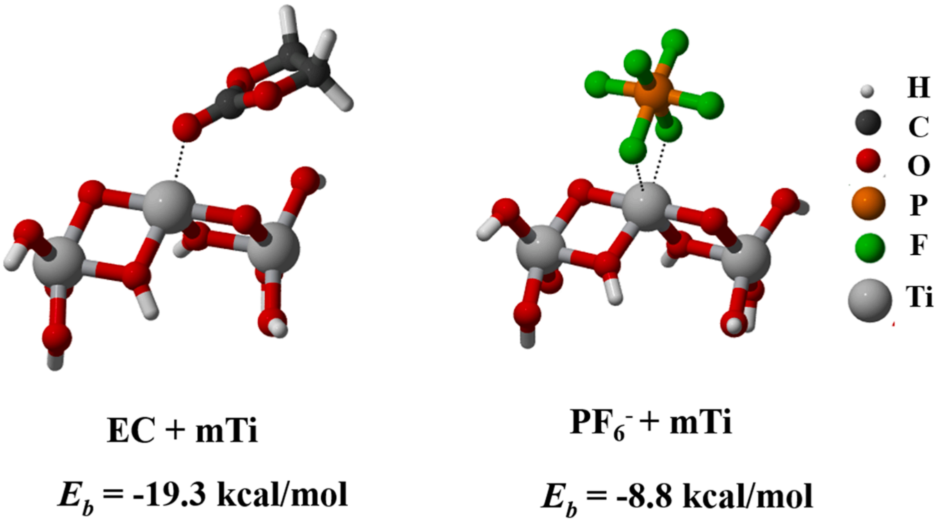

Fig. 5. Structures of adsorption products, Eb: binding energy of binding products; theoretical level: B3LYP-D3/def2-TZVP//B3LYP-D3/def2-SVP with SMD.

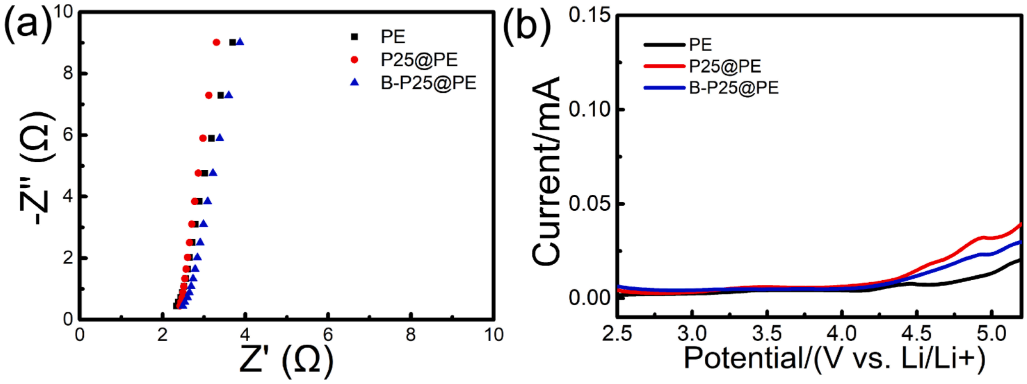

Fig. 6. (a) Impedance spectra of PE, P25@PE and B-P25@PE separators assembled in stainless steel symmetrical cells. (b) Linear sweep voltammetry plots of Li/SS based on PE, P25@PE and B-P25@PE separators.

And it means the modification of the oxygen vacancies of TiO_2 had no adverse effect on its thermal stability.

3.3. *Cells performance*

We assembled different separators in $LiFePO_4$ half-cell and tested their effects on electrochemical performance. Firstly, the cyclic voltammetry curves of the half cell with different separators were tested. As shown in Fig. S2, there was only a pair of redox peaks in the charge discharge range, corresponding to the Fe^{2+}/Fe^{3+} redox couple, which excluded the side reaction of TiO_2. The rate performance of $LiFePO_4$ half-cells equipped with different separators of PE, P25@PE and B-P25@PE is shown in Fig. 7a. Under different discharge current density (0.5C, 1C, 2C, 5C, 10C), the discharge capacity decreases with the increasing of current density. Under the condition of current density less than 2C, the discharge capacity of the three is basically no difference, that is, the discharge capacity is 143 $mAh·g^{-1}$(0.5C), 138 $mAh·g^{-1}$ (1C), 126 $mAh·g^{-1}$ (2C). At a current of 10C, the discharge capacity of the PE separator is significantly different from that of the ceramic separators, which is only 78 $mAh·g^{-1}$ (10C), less than the 84 $mAh·g^{-1}$ (10C) of the P25@PE separator and 91 $mAh·g^{-1}$ (10C) of the B-P25@PE separator. It is presumed that the concentration polarization increases the interface impedance, and the lithium ion concentration at the interface of the $LiFePO_4$ positive electrode material limits the reaction, resulting in a decrease in discharge capacity [11,26].

For the analysis of the specific conditions, we studied its capacity-voltage curve to help understand the differences. As shown in the Fig. 7b-d, as the discharge current increases, the discharge voltage platform of the $LiFePO_4$ half-cell decreases, accompanied by a decrease in discharge capacity, which is due to the increase in polarization caused by the current [26]. Among them, when the current is less than 2C, the discharge platform of the three are almost the same, 3.39 V (0.5C), 3.36 V (1C), 3.29 V (2C), so there is no difference in their discharge capacity. When the current increases to 5C, the difference of discharge platforms is shown. At 10C, the difference of the $LiFePO_4$ half-cell discharge platform is obvious, namely 2.71 V (PE), 2.89 V (P25@PE), 2.93 V (B-P25@PE), the increase in polarization causes differences in their discharge platforms, which ultimately leads to differences in discharge capacity. The addition of oxide interface layer helps to reduce polarization and reduce the loss of discharge capacity of $LiFePO_4$ at high current. Comparing P25 and B-P25, the introduction of oxygen vacancies on the oxide active layer promotes the desolvation of Li^+-EC and has a higher Li^+ migration rate, so it has a better capacity retention rate.

The discharge capacity and Coulombic efficiency of the $LiFePO_4$ half-cells equipped with different separators at a current density of 1C is shown in Fig. 8. It can be found that the $LiFePO_4$ half-cells equipped with different separators have a discharge capacity of 138 $mAh·g^{-1}$, and the Coulombic efficiency is close to 100%, which indicates that the oxide active layer hardly affects the charge and discharge performance of $LiFePO_4$ in the 100th cycle.

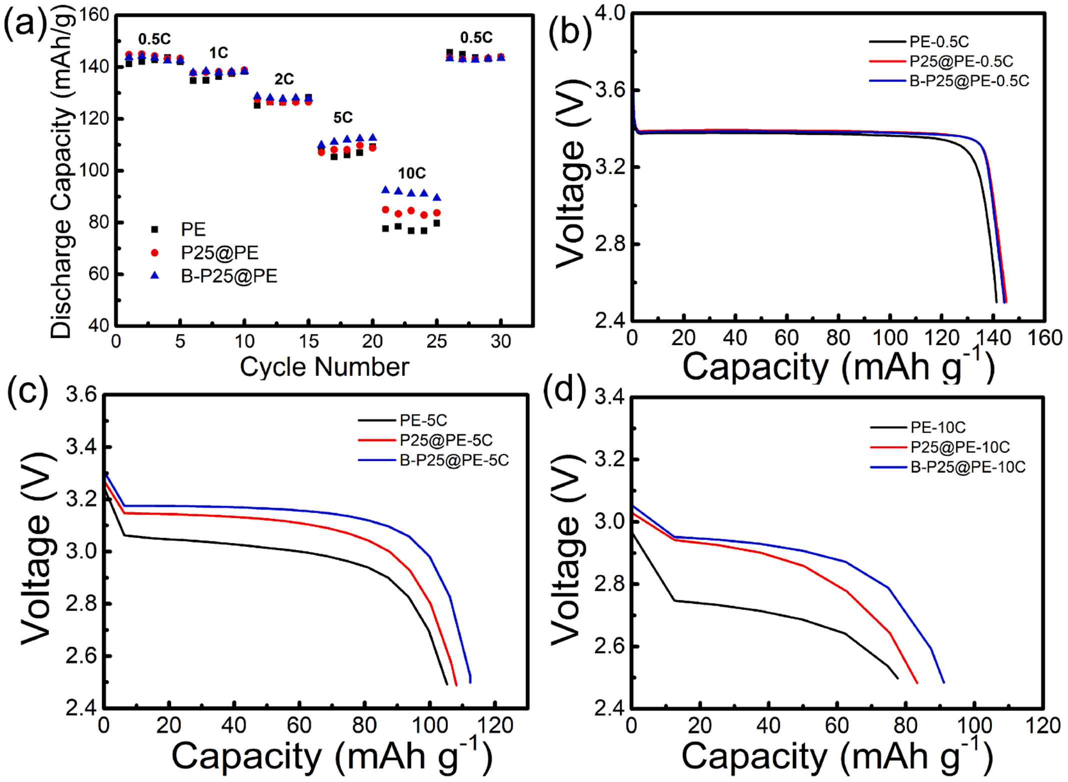

Fig. 7. (a) is the rate performance curve of PE, P25@PE and B-P25@PE separators assembled in $LiFePO_4$ half-cell under 0.5C, 1C, 2C, 5C and 10C currents; (b), (c) and (d) are the Voltage-capacity curves of PE, P25@PE and B-P25@PE separators assembled in $LiFePO_4$ half-cells under 0.5C, 5C and 10C currents, respectively.

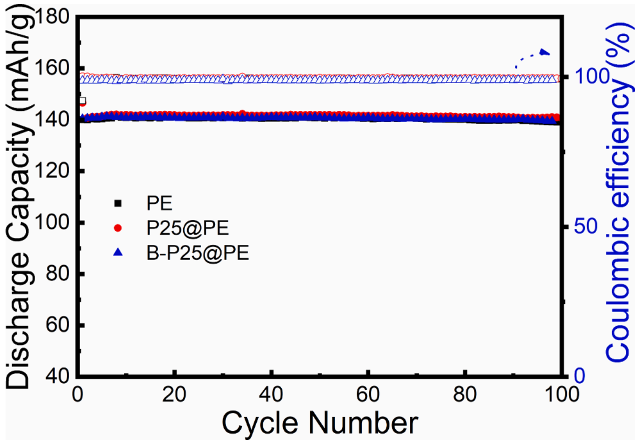

Fig. 8. Galvanostatic cycle performance curve of PE, P25@PE and B-P25@PE separators assembled in $LiFePO_4$ half-cell with 1C current.

4. Conclusions

TiO_2 nanoparticles with oxygen vacancies were prepared by $NaBH_4$ reduction method, and coated on the PE separator as an active layer to study its interaction with lithium ion electrolyte. B-P25 as an active layer improves the t_{Li^+}, from 0.28 to 0.50. Through infrared characterization and theoretical calculations, it is found that oxygen vacancies are more likely to adsorb EC molecules and indirectly promote the dissociation of Li^+-EC, so that partially solvated Li^+ has a stronger mobility and higher lithium ion conductivity, so it is assembled in $LiFePO_4$ half-cells has better rate performance.

CRediT authorship contribution statement

Xin Wang: Conceptualization, Methodology, Investigation, Data curation, Writing - original draft. **Haiming Hua:** Software, Data curation, Writing - original draft. **Longqing Peng:** Methodology, Investigation, Data curation. **Boyang Huang:** Investigation, Data curation. **Peng Zhang:** Conceptualization, Supervision. **Jinbao Zhao:** Conceptualization, Resources, Supervision.

Declaration of Competing Interest

The authors declare that they have no known competing financial interests or personal relationships that could have appeared to influence the work reported in this paper.

Acknowledgment

The authors gratefully acknowledge financial support from the National Natural Science Foundation of China (Grant Numbers 21875195), the Fundamental Research Funds for the Central Universities (Grant Number 20720190040) and the Key Project of Science and Technology of Fujian Province (2018H6019).

Appendix A. Supplementary material

Supplementary data to this article can be found online at https://doi.org/10.1016/j.apsusc.2020.148661.

References

[1] J.-M. Tarascon, M. Armand, Issues and challenges facing rechargeable lithium batteries, Nature 414 (6861) (2001) 359–367.
[2] M. Armand, J.-M. Tarascon, Building better batteries, Nature 451 (7179) (2008) 652–657.

[3] C. Shi, P. Zhang, L. Chen, P. Yang, J. Zhao, Effect of a thin ceramic-coating layer on thermal and electrochemical properties of polyethylene separator for lithium-ion batteries, J. Power Sources 270 (2014) 547–553.

[4] H.e. Chen, Q. Lin, Q. Xu, Y. Yang, Z. Shao, Y. Wang, Plasma activation and atomic layer deposition of TiO2 on polypropylene membranes for improved performances of lithium-ion batteries, J. Membr. Sci. 458 (2014) 217–224.

[5] P. Zhang, L. Chen, C. Shi, P. Yang, J. Zhao, Development and characterization of silica tube-coated separator for lithium ion batteries, J. Power Sources 284 (2015) 10–15.

[6] W. Luo, L. Zhou, K. Fu, Z. Yang, J. Wan, M. Manno, Y. Yao, H. Zhu, B. Yang, L. Hu, A thermally conductive separator for stable li metal anodes, Nano Lett. 15 (9) (2015) 6149–6154, https://doi.org/10.1021/acs.nanolett.5b02432.

[7] P. Yang, P. Zhang, C. Shi, L. Chen, J. Dai, J. Zhao, The functional separator coated with core–shell structured silica–poly(methyl methacrylate) sub-microspheres for lithium-ion batteries, J. Membr. Sci. 474 (2015) 148–155.

[8] J. Dai, C. Shi, C. Li, X. Shen, L. Peng, D. Wu, D. Sun, P. Zhang, J. Zhao, A rational design of separator with substantially enhanced thermal features for lithium-ion batteries by the polydopamine–ceramic composite modification of polyolefin membranes, Energy Environ. Sci. 9 (10) (2016) 3252–3261.

[9] J. Cho, Y.-C. Jung, Y.S. Lee, D.-W. Kim, High performance separator coated with amino-functionalized SiO2 particles for safety enhanced lithium-ion batteries, J. Membr. Sci. 535 (2017) 151–157.

[10] W. Xu, Z. Wang, L. Shi, Y. Ma, S. Yuan, L. Sun, Y. Zhao, M. Zhang, J. Zhu, Layer-by-layer deposition of organic–inorganic hybrid multilayer on microporous polyethylene separator to enhance the electrochemical performance of lithium-ion battery, ACS Appl. Mater. Interfaces 7 (37) (2015) 20678–20686, https://doi.org/10.1021/acsami.5b05457.

[11] R. Zahn, M.F. Lagadec, M. Hess, V. Wood, Improving ionic conductivity and lithium-ion transference number in lithium-ion battery separators, ACS Appl. Mater. Interfaces 8 (48) (2016) 32637–32642, https://doi.org/10.1021/acsami.6b12085.

[12] Z. Wang, F. Guo, C. Chen, L. Shi, S. Yuan, L. Sun, J. Zhu, Self-assembly of PEI/SiO 2 on polyethylene separators for li-ion batteries with enhanced rate capability, ACS Appl. Mater. Interfaces 7 (5) (2015) 3314–3322, https://doi.org/10.1021/am508149n.

[13] M.K. Nowotny, L.R. Sheppard, T. Bak, J. Nowotny, Defect chemistry of titanium dioxide. Application of defect engineering in processing of TiO 2 -based photocatalysts, J. Phys. Chem. C 112 (14) (2008) 5275–5300, https://doi.org/10.1021/jp077275m.

[14] Q. Sun, D. Cortie, S. Zhang, T.J. Frankcombe, G. She, J. Gao, L.R. Sheppard, W. Hu, H. Chen, S. Zhuo, D. Chen, R.L. Withers, G. McIntyre, D. Yu, W. Shi, Y. Liu, The formation of defect-pairs for highly efficient visible-light catalysts, Adv. Mater. 29 (11) (2017) 1605123, https://doi.org/10.1002/adma.201605123.

[15] N.J. Lawrence, J.R. Brewer, L.u. Wang, T.-S. Wu, J. Wells-Kingsbury, M.M. Ihrig, G. Wang, Y.-L. Soo, W.-N. Mei, C.L. Cheung, Defect engineering in cubic cerium oxide nanostructures for catalytic oxidation, Nano Lett. 11 (7) (2011) 2666–2671, https://doi.org/10.1021/nl200722z.

[16] X. Chen, L. Liu, F. Huang, Black titanium dioxide (TiO 2) nanomaterials, Chem. Soc. Rev. 44 (7) (2015) 1861–1885.

[17] Q. Kang, J. Cao, Y. Zhang, L. Liu, H. Xu, J. Ye, Reduced TiO2 nanotube arrays for photoelectrochemical water splitting, J. Mater. Chem. A 1 (18) (2013) 5766, https://doi.org/10.1039/c3ta10689f.

[18] J. Chen, Z. Ding, C. Wang, H. Hou, Y. Zhang, C. Wang, G. Zou, X. Ji, Black anatase titania with ultrafast sodium-storage performances stimulated by oxygen vacancies, ACS Appl. Mater. Interfaces 8 (14) (2016) 9142–9151, https://doi.org/10.1021/acsami.6b01183.

[19] G. Ou, Y. Xu, B. Wen, R. Lin, B. Ge, Y. Tang, Y. Liang, C. Yang, K. Huang, D. Zu, R. Yu, W. Chen, J. Li, H. Wu, L.-M. Liu, Y. Li, Tuning defects in oxides at room temperature by lithium reduction, Nat. Commun. 9 (2018), https://doi.org/10.1038/s41467-018-03765-0.

[20] R. Ren, Z. Wen, S. Cui, Y. Hou, X. Guo, J. Chen, Controllable Synthesis and Tunable Photocatalytic Properties of Ti3+-doped TiO2, Sci. Rep. 5 (1) (2015), https://doi.org/10.1038/srep10714.

[21] J. Evans, C.A. Vincent, P.G. Bruce, Electrochemical measurement of transference numbers in polymer electrolytes, Polymer 28 (13) (1987) 2324–2328.

[22] P.J. Stephens, F.J. Devlin, C.F. Chabalowski, M.J. Frisch, Ab initio calculation of vibrational absorption and circular dichroism spectra using density functional force fields, J. Phys. Chem. 98 (45) (1994) 11623–11627, https://doi.org/10.1021/j100096a001.

[23] A.V. Marenich, C.J. Cramer, D.G. Truhlar, Universal solvation model based on solute electron density and on a continuum model of the solvent defined by the bulk dielectric constant and atomic surface tensions, J. Phys. Chem. B 113 (18) (2009) 6378–6396, https://doi.org/10.1021/jp810292n.

[24] X. Mao, L. Shi, H. Zhang, Z. Wang, J. Zhu, Z. Qiu, Y. Zhao, M. Zhang, S. Yuan, Polyethylene separator activated by hybrid coating improving Li+ ion transference number and ionic conductivity for Li-metal battery, J. Power Sources 342 (2017) 816–824.

[25] Y. Zhang, J.-J. Yuan, Y.-Z. Song, X. Yin, C.-C. Sun, L.-P. Zhu, B.-K. Zhu, Tannic acid/polyethyleneimine-decorated polypropylene separators for Li-Ion batteries and the role of the interfaces between separator and electrolyte, Electrochim. Acta 275 (2018) 25–31.

[26] K.M. Diederichsen, E.J. McShane, B.D. McCloskey, Promising routes to a high Li + transference number electrolyte for lithium ion batteries, ACS Energy Lett. 2 (11) (2017) 2563–2575, https://doi.org/10.1021/acsenergylett.7b00792.

[27] K.L. Mathews, A.M. Budgin, S. Beeram, A.T. Joenathan, B.D. Stein, U. Werner-Zwanziger, M. Pink, L.A. Baker, W.E. Mahmoud, J.P. Carini, L.M. Bronstein, Solid polymer electrolytes which contain tricoordinate boron for enhanced conductivity and transference numbers, J. Mater. Chem. A 1 (4) (2013) 1108–1116.

[28] R. Aroca, R. Nazri, G.A. Nazri, A.J. Camargo, M. Trsic, Vibrational spectra and ion-pair properties of lithium hexafluorophosphate in ethylene carbonate based mixed-solvent systems for lithium batteries, J. Solution Chem. 29 (2000) 1047–1060, https://doi.org/10.1023/a:1005151220893.

[29] S. Bertilsson, F. Larsson, M. Furlani, I. Albinsson, B.-E. Mellander, Lithium-ion battery electrolyte emissions analyzed by coupled thermogravimetric/Fourier-transform infrared spectroscopy, J. Power Sources 365 (2017) 446–455.

[30] T. Hou, G. Yang, N.N. Rajput, J. Self, S.-W. Park, J. Nanda, K.A. Persson, The influence of FEC on the solvation structure and reduction reaction of LiPF6/EC electrolytes and its implication for solid electrolyte interphase formation, Nano Energy 64 (2019) 103881, https://doi.org/10.1016/j.nanoen.2019.103881.

[31] K. Hongyou, T. Hattori, Y. Nagai, T. Tanaka, H. Nii, K. Shoda, Dynamic in situ fourier transform infrared measurements of chemical bonds of electrolyte solvents during the initial charging process in a Li ion battery, J. Power Sources 243 (2013) 72–77.

[32] H.-S. Jeong, S.-Y. Lee, Closely packed SiO2 nanoparticles/poly(vinylidene fluoride-hexafluoropropylene) layers-coated polyethylene separators for lithium-ion batteries, J. Power Sources 196 (16) (2011) 6716–6722.